Local strain measurement in tensile test of Al/steel dissimilar friction stir weld using digital image correlation

Yoshihiko Uematsu (yuematsu@gifu-u.ac.jp)
Gifu University
Toshifumi Kakiuchi
Gifu University
Kenta Niimi
Gifu University
Paul Dario Toasa Caiza
Karlsruhe Institute of Technology

Research Article

Keywords: Friction stir welding, Dissimilar weld, Local strain, Digital image correlation, Aluminium alloy, Stainless steel

Posted Date: May 7th, 2021

DOI: https://doi.org/10.21203/rs.3.rs-421146/v1

Abstract

A6061-T6 aluminum alloy plate was butt welded to type 304 stainless steel plate by a friction stir welding (FSW) technique to fabricate a dissimilar weld. Subsequently, digital image correlation (DIC) analysis was performed on the dissimilar weld to investigate the local deformation behavior near the joint interface under a tensile loading condition. The normal strain in the loading direction concentrated near the interface on both top and bottom surfaces. The positions of the strain-concentrated areas were different on both sides; around 9 mm away from the interface on the top surface and 6 mm away on the bottom surface, which could be attributed to the local softening developed during the FSW process.

1. Introduction

Multi-material design concept is becoming common especially in the automotive industries, whilst joining of dissimilar materials is essential to achieve that design concept. Consequently, joining of dissimilar alloys have been widely tried. The solid state joining process, friction stir welding (FSW), is expected to be a joining method between aluminium (Al) alloy and steel plates, which are two major materials consisting of car body components. Therefore, there have been many trials for joining Al alloys and steels by FSW [1-7] and friction stir spot welding (FSSW) [8-10] techniques. The optimization of welding parameters and the microstructure analysis at the interface between Al and steel have been widely investigate, focusing on the development of intermetallic compounds (IMC) along the interface [11-13]. That is because IMC layer plays an important role for achieving good joint strengths. Recently, micro-sized specimens were sampled near the interface, and the interface joint strengths were directly measured [14-16], which revealed that the high performance of interface strength between A6061-T6 and type 304 stainless steel was achieved when the thickness of IMC layer was less than 0.4 μm [14].

In our previous study [17], residual stresses in Al/steel dissimilar friction stir weld were measured and the effect of post heat treatment was discussed. In Al/steel dissimilar welds, local deformation behaviour near the interface might be complex because elastic moduli are largely different between Al and steel. Therefore, in this study, we focused on a digital image correlation (DIC) method, which can measure the displacement using two digital images before and after loading. DIC has been used for the local displacement measurement of weldments [18], friction stir welds [19-21] or spot welds [22] and friction stir dissimilar welds of different Al alloys [23]. For example, the hardness distribution in the weld zone is asymmetric between top and bottom sides, and retreating and advancing sides in FSW joints. DIC measurement during tensile test revealed that the local strain concentration at the locally-softened area resulted in the final tensile failure [21]. Although Al/steel dissimilar welds have more significant discontinuity at the interface compared with Al/Al similar or Al/Al dissimilar welds, the DIC analysis of Al/steel dissimilar weld has not been caried out. Consequently, Al alloy and steel plates were joined by an FSW technique, and the local strain near the interface was measured by a DIC method on both top and bottom surfaces to investigate the effect of discontinuity of microstructures and elastic moduli on the local deformation behaviour.

2. Experiment Details

2.1 Materials and welding conditions

The materials used are Al alloy, A6061-T6, and stainless steel, type 304, plates with the width of 75 mm and length of 150 mm. The thicknesses of A6061 and type 304 plates are 6 and 5 mm, respectively. The tool with concave shoulder, with a diameter of 14 mm, was used for the joining. The tool has a threaded probe with the diameter of 6 mm and length of 4.7 mm. The tool rotational and traveling speeds were fixed at 700 rpm and 100 mm/min, respectively. The tool plunge depth and tool-to-workpiece angle were 0.8 mm and 3° from the vertical axis, respectively. The detailed joining procedures and microstructures in the stir zone (SZ) are described in our previous studies [6,17].

2.2 Experimental Procedures

The depth of 0.1 mm was removed from the top and bottom surfaces of the as-welded plate by milling as schematically shown in Fig. 1. Subsequently, the tensile specimens were sampled from the welded plates by electrical discharge machining. Tensile tests were conducted using the specimens in accordance with JIS (Japanese Industrial Standard) Z 2241 13B, where the test piece has the gauge length of 50 mm and the width of 12.5 mm as shown in Fig. 2. The tool centre corresponds to the centre of the gauge length of the tensile specimen. Tensile tests were conducted using an electro-hydraulic testing machine (SHIMADZU: EHF-LV-020k1-020).

A digital camera, Nikon D7500, with the CMOS sensor with the size of 23.5 × 15.7 mm was used for the DIC procedures, in which images of specimen surfaces were sampled. The lens of the digital camera was Nikon AF-S VR Micro-Nikkor 105 mm f/2.8G IF-FD. Random dotted patterns on the specimen surfaces were formed by white and black colour sprays. In the DIC procedure, deformation is measured by the matching of luminance distribution in the subset areas before and after loading. The example of random dotted pattern and the subset area are shown in Fig. 3.

3. Results

3.1 Hardness distribution

The detailed microstructures and mechanical properties are described elsewhere [6,17], thus the hardness distribution is briefly shown in this section. Figure 4 shows the hardness profiles measured on the top and bottom surfaces of the tensile specimen along the dotted line in Fig. 2. Softening occurred in the SZ due to the heat input during FSW, and the minimum hardness appeared at the thermo-mechanically affected zone (TMAZ). It should be noted that the minimum hardness appears at about 9 mm away from the interface on the top surface and about 6.5 mm on the bottom surface. In addition, the hardness near the interface (0~1 mm) on the bottom surface was nearly comparable to the minimum hardness at 6.5 mm away from the interface. The hardness mapping measured on the side surface of Al side is shown in Fig. 5 [6]. It should be noted that the area of lower hardness (blue area) in the TMAZ has vertical

asymmetricity, where lower hardness appears further from the interface on the top side. Furthermore, minimum hardness appears near the interface (0~3 mm) only on the bottom side.

3.2 DIC analysis: Top and bottom surfaces

The ultimate tensile failure load of the joint was 201 MPa, where tensile failure occurred in Al side along TMAZ as shown in Fig. 6, indicating that the interface strength was higher than the TMAZ with lower hardness [6]. Firstly, DIC analysis was performed on the top surface of the dissimilar weld of the tensile specimen. Figure 7 shows the analytical area on the top surface including the interface between Al and steel, where *y* axis corresponds to the loading direction. The analytical conditions are summarized in Table 1. The image before loading was used as a reference image, and the images at 4.0 kN (86 MPa), 5.0 kN (107 MPa) and 6.0 kN (128 MPa) are used for the DIC analysis. The DIC analytical results showing *y*-axis displacement and strain are revealed in Fig. 8. Figure 9 shows the *y*-axis strain along the dotted line in Fig. 8(b) at 6.0 kN. It should be noted that the maximum local strain concentration occurred at about 9 mm away from the interface, which corresponds to the locally-softened area of TMAZ as shown in Fig. 4. The local strain distributions at 0, 1, 9, 12 and 14 mm away from the interface are shown in Fig. 10. The areas in the figure were squares with the size of 1.85 mm × 1.85 mm. At the beginning of the loading (4.0 kN and 5.0 kN), strain concentration occurred at about 1 mm away from the interface in very narrow area. However, the wide strain concentration occurred at 9 mm from the interface at 6.0 kN, which corresponds to the softened TMAZ (Fig. 4) and the actual fracture location (Fig. 6).

Subsequently, DIC analysis was performed on the bottom surface, where the analytical conditions are summarized in Table 1. *y*-axis displacement and strain are shown in Fig 11. Furthermore, the local strain distributions at 0, 3, 5.6, 11.5 and 19 mm away from the interface are shown in Fig. 12. Local strain concentration occurred just beside the interface from 4.0 to 6.0 kN, while large strain occurred at about 5.6 mm away from the interface at 6.0 kN. That location corresponds to the locally-softened area (Fig. 4) and the actual fracture location (Fig. 6). Consequently, the local strain concentration occurred at the locally-softened area in TMAZ, and just beside the interface on the bottom surface.

The DIC analytical result on the side surface is shown in Fig. 13 as the strain distribution at 6.0 kN. It should be noted that the strain asymmetricity between top and bottom sides is observed on the side surface along TMAZ. In addition, local strain concentration near the interface occurred only on the bottom side as shown by the arrow in the figure, and it is consistent with Figs.10 and 12. In our previous study, the strain distribution was measured by DIC using friction stir welded Al-Mg-Sc plates. In that case, local strain concentration occurred only at TMAZ where minimum hardness appeared, and static failure occurred at the maximum straining area. In the present case, local straining occurred at TMAZ and just beside the interface on the bottom side. However, local straining area was much narrower near the interface due to the constraint by steel with higher elastic modulus. Therefore, it is assumed that the final failure predominantly occurs at wider local-straining area in TMAZ.

3.3 Local stress-strain curves

The local straining figures shown in Figs. 10 and 12 were obtained at every 0.5 kN on the top surface, and every 1 kN on the bottom surface to draw local stress-strain curves. The local strain was defended as the average value of each square shown in Figs. 10 and 12. Figures 14a and 14b are the local stress-strain curves at SZ, TMAZ, HAZ and base metal (BM) on the top and bottom surfaces, respectively. The black solid line is a stress-strain curve of the bulk sample of the base metal, where elastic modulus of 68.3 GPa was measured by DIC in the present study and 0.2% proof stress of 287 MPa was given by a material supplier. On the top surface (Fig. 14a), the stress-strain relationships in SZ, HAZ and BM are linear, where the local elastic moduli are 65.4, 53.5 and 54.0 GPa, respectively. On the other hand, local yielding occurred only at TMAZ, where the hardness was minimum. The elastic modulus at TMAZ is 60.8 GPa. The local 0.2% proof stress at TMAZ is estimated about 120 MPa, which is 58 % lower than the base metal. The hardness drop at TMAZ was about 48 % as shown in Fig. 4, therefore the drop of local yield stress was larger than the hardness. However, the value of the local yield stress still seems reasonable because the deference in the reduction rates is small. Similar to the top surface, the local yielding is prominent only at TMAZ on the bottom surface (Fig. 14b), where the local proof stress is also about 120 MPa. The strain value at the maximum load of 6.0 kN is also slightly larger than the elastic line at SZ, but it seems a measurement error because the strain values at the maximum load on the bottom side are larger than the top side at all locations including base metal. The local elastic moduli at SZ, TMAZ, HAZ and BM on the bottom side are 63.8, 50.7, 52.9 and 60.6, respectively. It should be noted that the elastic modulus at the SZ was the largest on both top and bottom surfaces. It was confirmed that many steel fragments were dispersed in the SZ by microstructural observations [6,17]. Therefore, higher local elastic modulus at the SZ could be attributed to such steel fragments with higher elastic modulus than Al.

4. Conclusions

Aluminium alloy, A6061-T6, plate was welded to type 304 stainless steel plate by a friction stir welding technique. The tensile tests were performed and the local straining behaviour near the interface between Al and steel was analysed by a digital image correlation (DIC) method. The main results obtained are as follows.

1. The hardness measurement revealed that local softening occurred in the SZ, TMAZ and HAZ. The asymmetricity of hardness distribution was recognized in the thickness direction. The minimum hardness appeared at TMAZ.
2. The maximum local strain concentration occurred at 9 mm and 6 mm away from the interface on top and bottom surfaces, respectively. The locations of this local strain concentration corresponded to those where minimum hardness appeared, namely TMAZ.
3. The maximum local strain concentration also appeared just beside the interface on the bottom surface, whilst the width of local strain concentration was narrower compared with that at TMAZ. Consequently, final tensile failure occurred along TMAZ, where local strain concentration area was much wider.

4. The local stress-strain curves at the SZ, TMAZ, HAZ and base metal were obtained using local images. The local yielding occurred only at TMAZ. The local elastic modulus at SZ was the highest because many steel fragments were dispersed in the SZ.

Declarations

Authors' contributions Y. Uematsu, T. Kakiuchi and K. Niimi planed and conducted fatigue tests and DIC analyses. PD. Toasa Caiza optimized DIC conditions. All authors discussed the results and contributed to the final manuscript.

References

1. Jiang WH. Kovavevic. Feasibility study of friction stir welding of 6061–T6 aluminium alloy with AISI 1018 steel. J Eng Manuf 2004;208(10):1323–1331.
2. Xiong JT, Li JL, Qian JW, Zhang FS, Huang WD. High strength lap joint of aluminium and stainless steels fabricated by friction stir welding with cutting pin. Sci Technol Weld Join. 2012;17(3):196–201.
3. Uematsu Y, Kakiuchi T, Kondoh E, Tozaki Y, Ibrahim I. Fatigue behavior of dissimilar A6061/rolled steel (SS400) friction stir welds. Quarterly J Jap Weld Soc. 2013;31(2):112–118.
4. Lan S, Liu X, Ni J. Microstructural evolution during friction stir welding of dissimilar aluminum alloy to advanced high-strength steel. Int J Adv Manuf Technol. 2016;82:2183–2193.
5. Patterson EE, Hovanski Y, P.Field D. Microstructural characterization of friction stir welded aluminum-steel joints. Metall Mater Trans A. 2016;47:2815–2829
6. Ogawa D, Kakiuchi T, Hashiba K, Uematsu Y. Mechanical properties of tailor welded Al/steel blanks made by friction stir welding and the effect of post heat treatment. Quarterly J Jap Weld Soc. 2018;36(3):160–166. (in Japanese)
7. Wang T, Sidhar H, Mishra RS, Hovanski Y, Upadhyay P, Carlson B. Effect of hook characteristics on the fracture behaviour of dissimilar friction stir welded aluminium alloy and mild steel sheets. Sci Technol Weld Join. 2019;24(2):178–184.
8. Liyanage T, Kilbourne J, Gerlich AP, North TH. Joint formation in dissimilar Al alloy/steel and Mg alloy/steel friction stir spot welds. Sci Technol Weld Join. 2009;14(6):500–508.
9. Uematsu Y, Tokaji K, Tozaki Y. Fatigue behaviour of dissimilar friction stir spot welds between A6061-T6 and low carbon steel sheets welded by a scroll grooved tool without probe. Fatigue Fract Eng Mater Struct. 2011;34(8):581–591.
10. Chen K, Liu X, Ni J. Keyhole refilled friction stir spot welding of aluminum alloy to advanced high strength steel. J Mater Process Tech. 2017;249:452–462.
11. Springer H, Kosta A, Santos JF, Raabe D. Influence on intermetallic phases and Kirkendall-porosity on the mechanical properties of joints between steel and aluminium alloys. Mater Sci Eng A. 2011;528:4630–4642.

12. Das H, Ghosh RN, Pal TK. Study on the formation and characterization of the intermetallics in friction stir welding of aluminum alloy to coated steel sheet lap joint. Metall Mater Sci Trans A. 2014;45:5098–5106.
13. Liu FC, Dong P. From thick intermetallic to nanoscale amorphous phase at Al-Fe joint interface: roles of friction stir welding conditions. Scripta Materialia. 2021;191:167–172.
14. Hatano R, Ogura T, Matsuda T, Sano T, Hirose A. Relationship between intermetallic compound layer thickness with deviation and interfacial strength for dissimilar joints of aluminum alloy and stainless steel. Mater Sci Eng A. 2018;735:361–366.
15. Matsuda T, Hatano R, Ogura T, Suzuki R, Shoji H, Sano T, Ohata M, Hirose A. Effect of mismatch in mechanical properties on interfacial strength of aluminum alloy/steel dissimilar joints. Mater Sci Eng A. 2020;786:139437.
16. Matsuda T, Sano T, Munekane M, Ohata M, Hirose A. Microscale tensile test of galvannealed steel/aluminum dissimilar joint for estimation of intrinsic interfacial strength. Scripta Materialia. 2020;186:196–201.
17. Ogawa D, Kakiuchi T, Hashiba K, Uematsu T. Residual stress measurement of Al/steel dissimilar friction stir weld. Sci Technol Weld Join. 2019;24(8):685–694.
18. Pérez Fernándes JÁ, Coppieters S, Debruyne D. Application of digital image correlation for the study of strain concentrations due to change in geometry in weld beads: parent interface of structural steel welds. Residual stress and microstructure effects on fatigue crack growth in AA2050 friction stir welds. Sci Technol Weld Join. 2016;21(8):670–679.
19. Wang FF, Li WY, Shen J, Zhang ZH, Li JL, Santos JF. Global and local mechanical properties and microstructure of Bobbin tool friction-stir-welded Al-Li alloy. Sci Technol Weld Join. 2016;21(6):479–483.
20. Niu P, Li W, Yang X, Vairis A. Effects of microstructural asymmetries across friction stir welded AA2024 joints on mechanical properties. Sci Technol Weld Join. 2018;23(1):58–62.
21. Besel Y, Besel M, Dietrich E, Wischek J, Mercado UA, Kakiuchi T, Uematsu Y. Heterogeneous local straining behavior under monotonic and cyclic loadings in a friction stir welded aluminum alloy. Int J Fatigue. 2019;125:138–148.
22. Herbelot C, Hoang TD, Imad A, Benseddiq N. Damage mechanisms under tension shear loading in friction stir spot welding. Sci Technol Weld Join. 2010;15(8):688–693.
23. Simar A, Jonckheere C, Deplus K, Pardoen T, Meester B. Comparing similar and dissimilar friction stir welds of 2017-6005A aluminium alloys. Sci Technol Weld Join. 2010;15(3):254–259.

Table

Table 1 DIC conditions.

	Top surface	Bottom surface	Side surface
Camera image area pixel × pixel	3712 × 5568		
Calibration value µm/pixel	5.13	7.01	7.5
Analytical area pixel × pixel (mm × mm)	2460 × 4106 (12.62 × 21.06)	1700 × 3400 (11.92 × 23.48)	350 × 3070 (2.63 × 23.03)
Subset area pixel × pixel (mm × mm)	55 × 55 (0.28 × 0.28)	55 × 55 (0.39 × 0.39)	55 × 55 (0.41 × 0.41)
Subset interval pixel (µm)	10 (51.3)	10 (70.1)	10 (75)

Figures

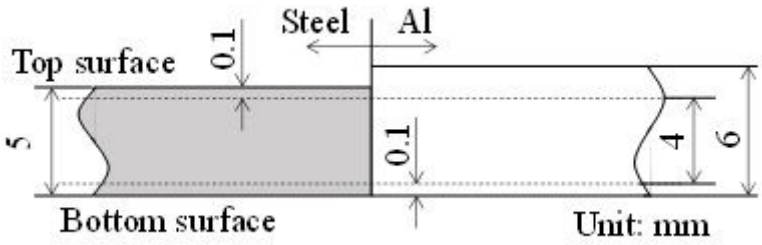

Figure 1

Schematic illustration showing a surface removal process.

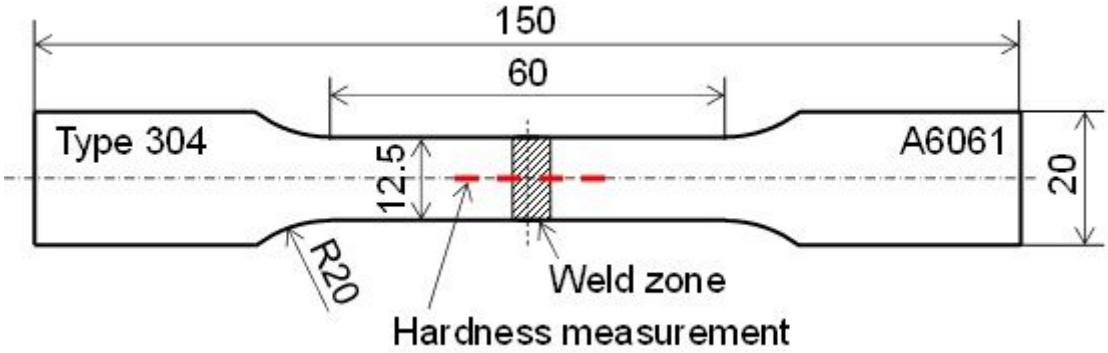

Figure 2

Tensile specimen configuration.

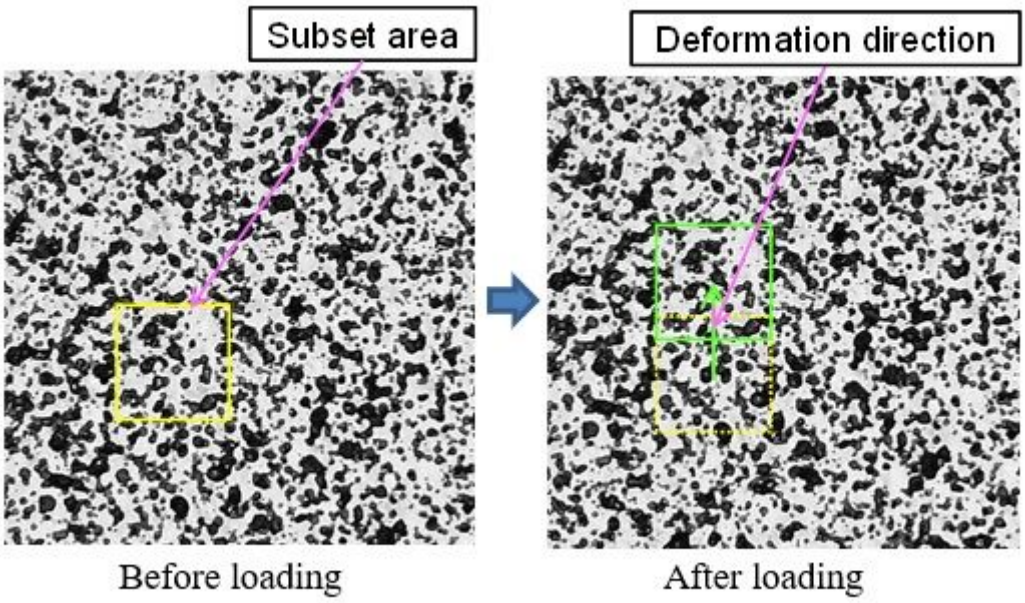

Figure 3

Schematic illustration of random dotted pattern and subset area .

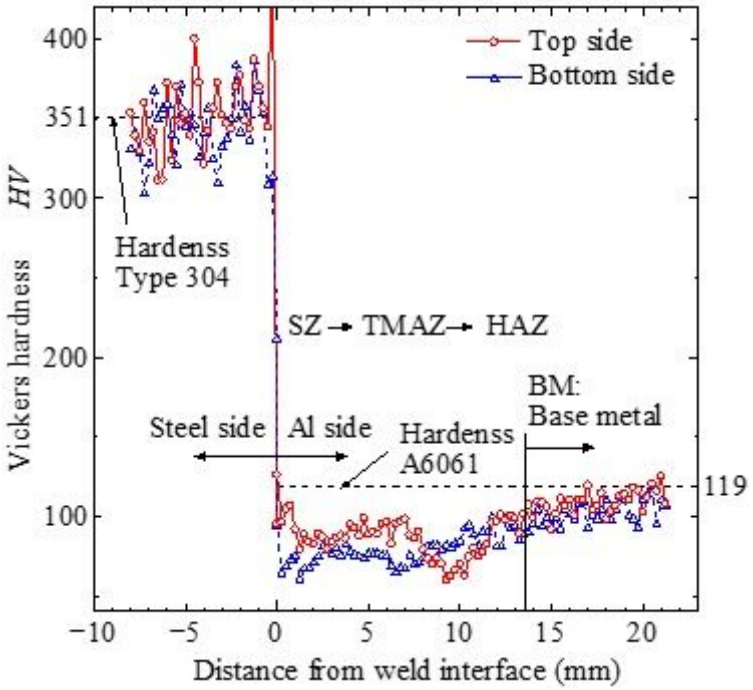

Figure 4

Hardness profiles on top and bottom surfaces.

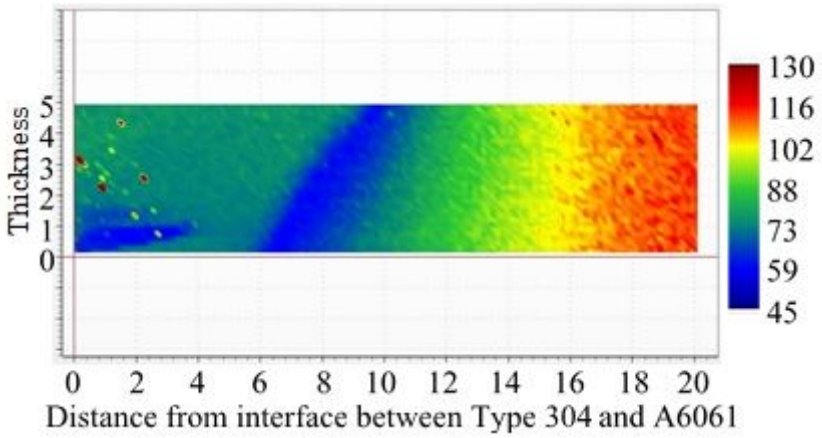

Figure 5

Hardness mapping measured on the side surface of Al side [6].

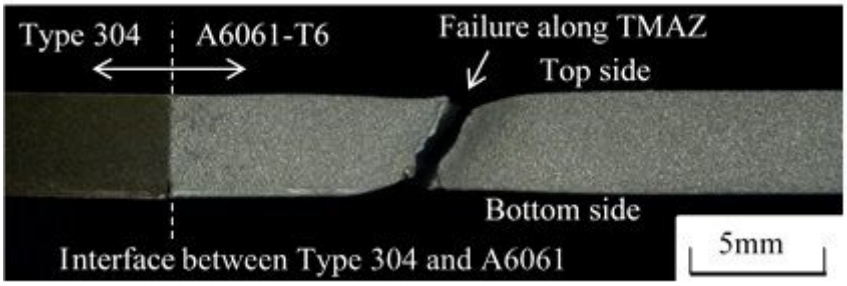

Figure 6

Tensile failure along TMAZ of Al-Steel joint (side view) [6].

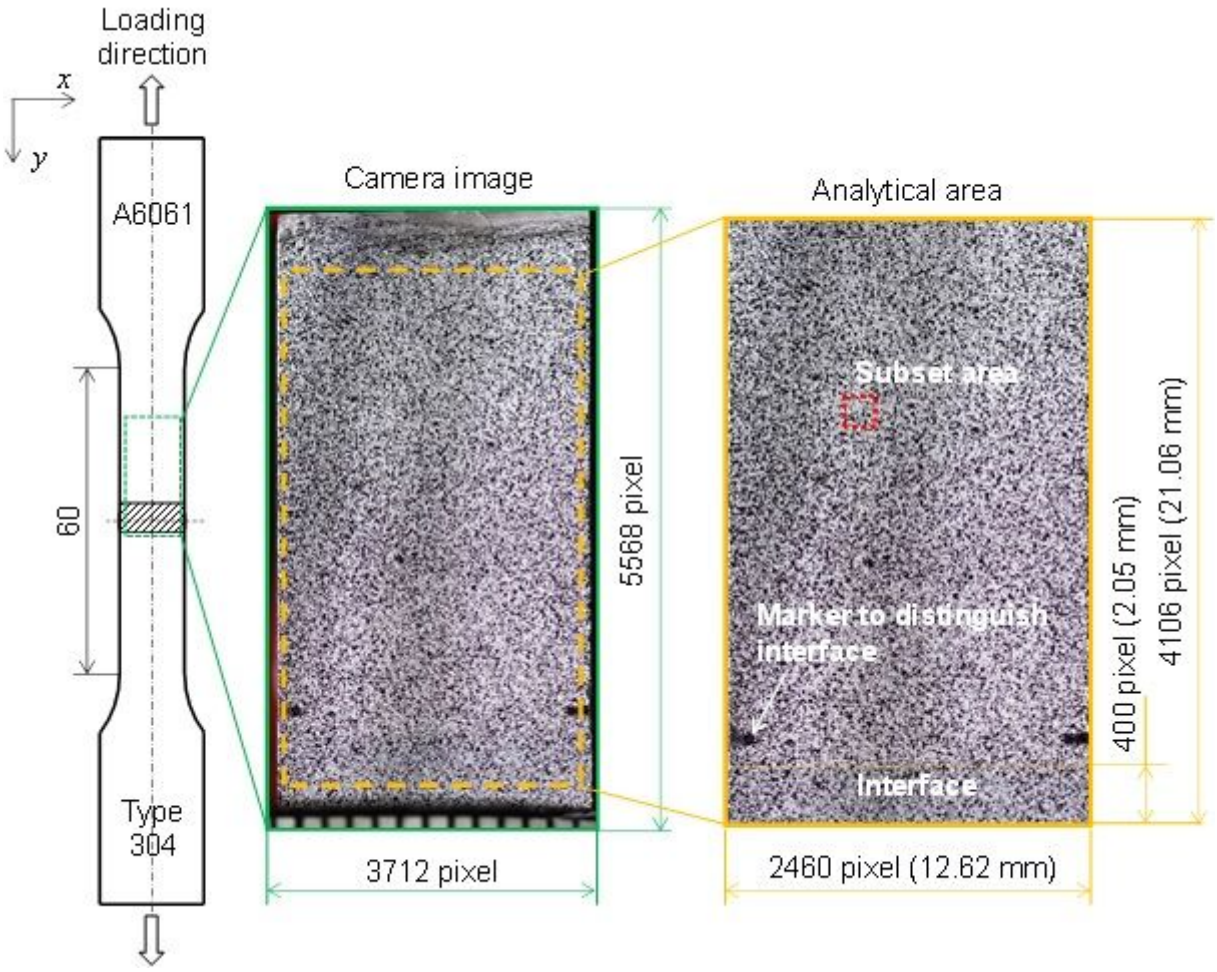

Figure 7

Schematic diagram showing analytical area on the top surface.

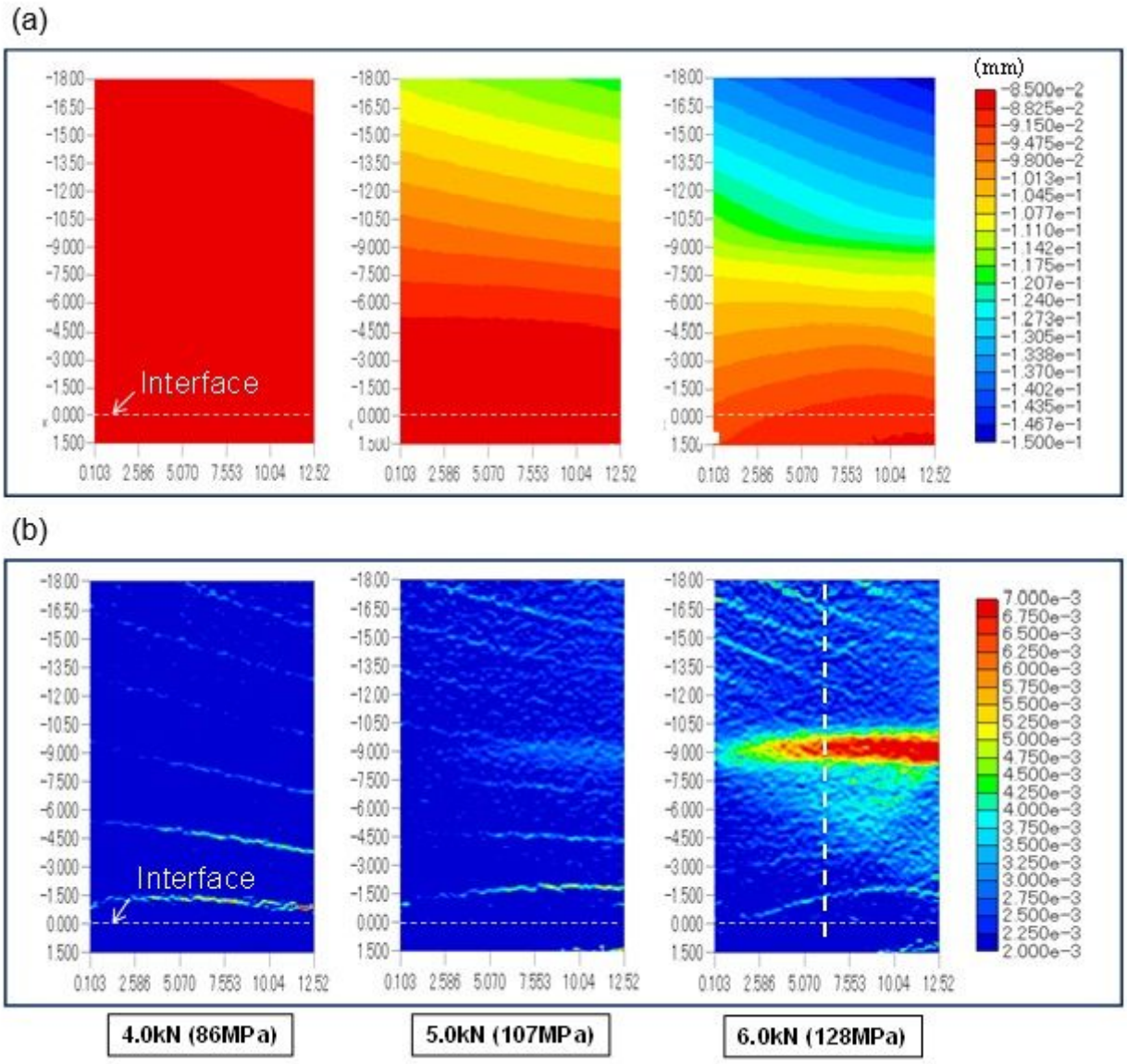

Figure 8

DIC results on the top surface at 4.0, 5.0 and 6.0 kN; (a) y-axis displacement, (b) y-axis strain.

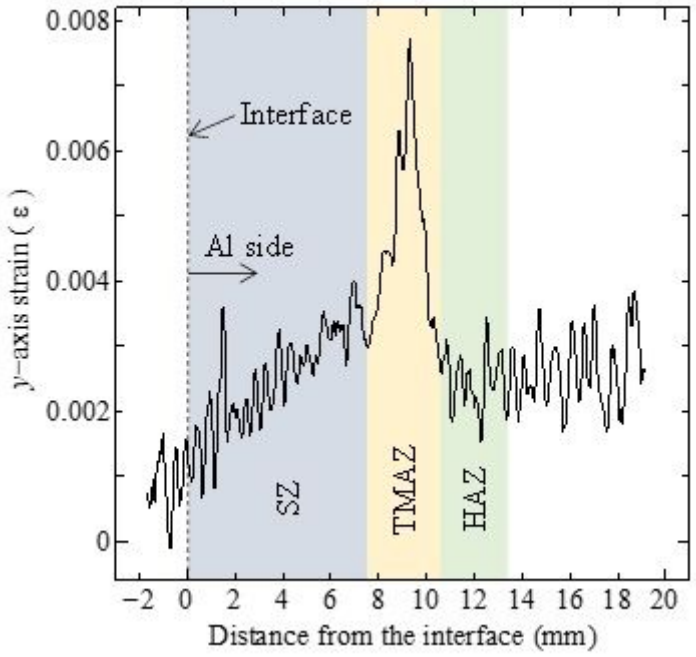

Figure 9

Strain distribution along the dotted line in Fig. 8(b) at 6.0 kN.

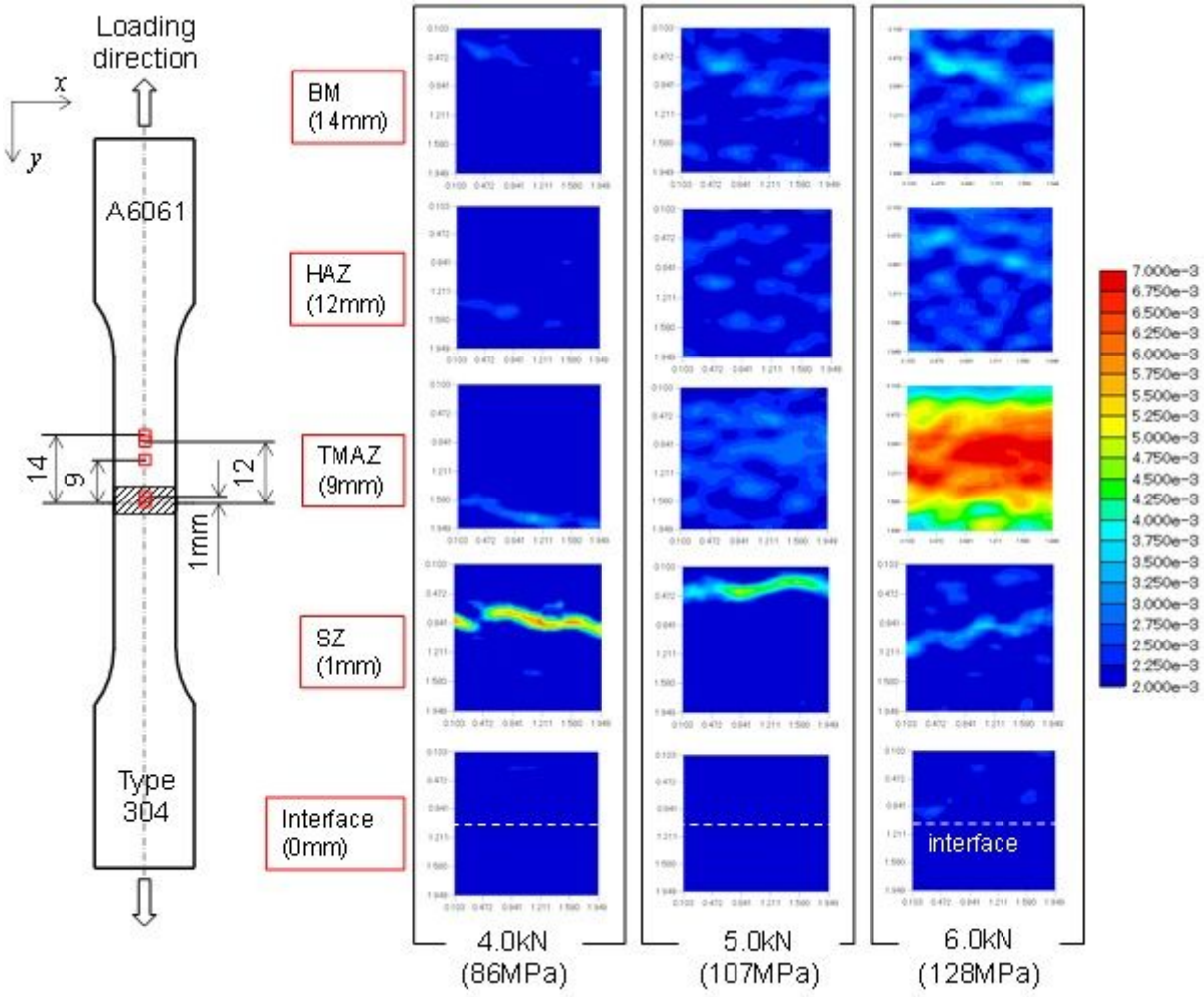

Figure 10

Local strain distribution on top surface at 4.0, 5.0 and 6.0 kN.

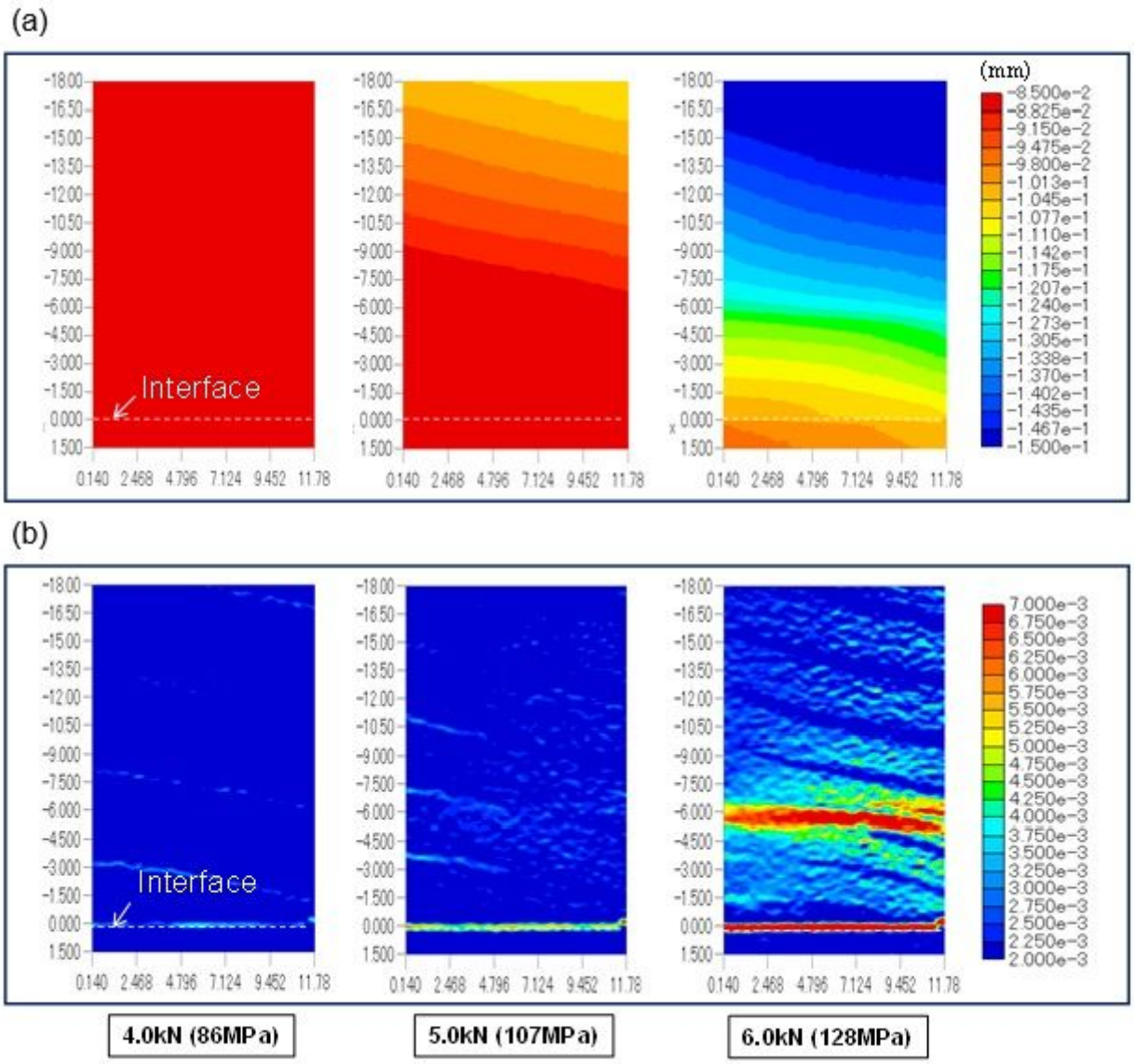

Figure 11

DIC results on the bottom surface at 4.0, 5.0 and 6.0 kN; (a) y-axis displacement, (b) y-axis strain.

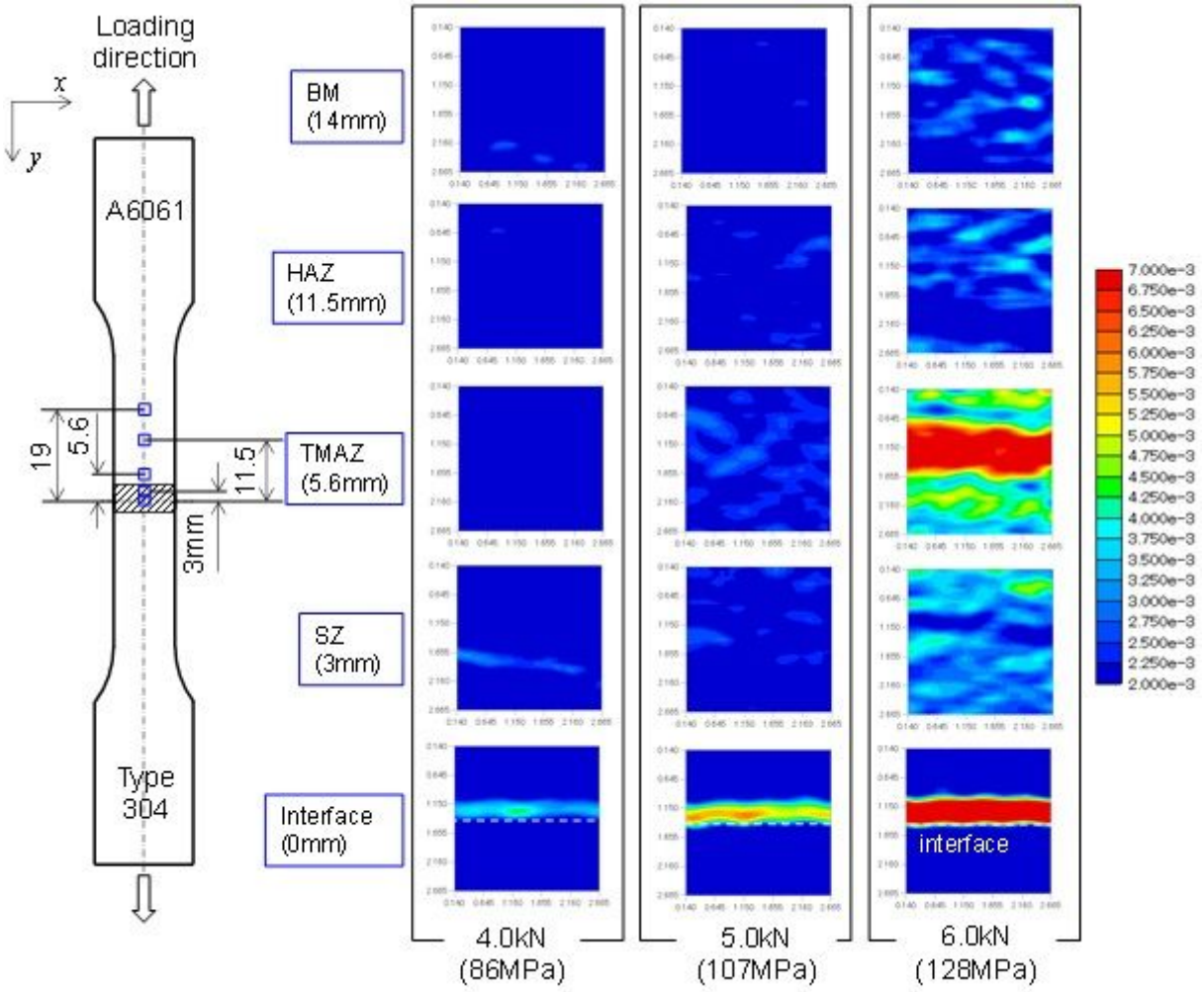

Figure 12

Local strain distribution on bottom surface at 4.0, 5.0 and 6.0 kN.

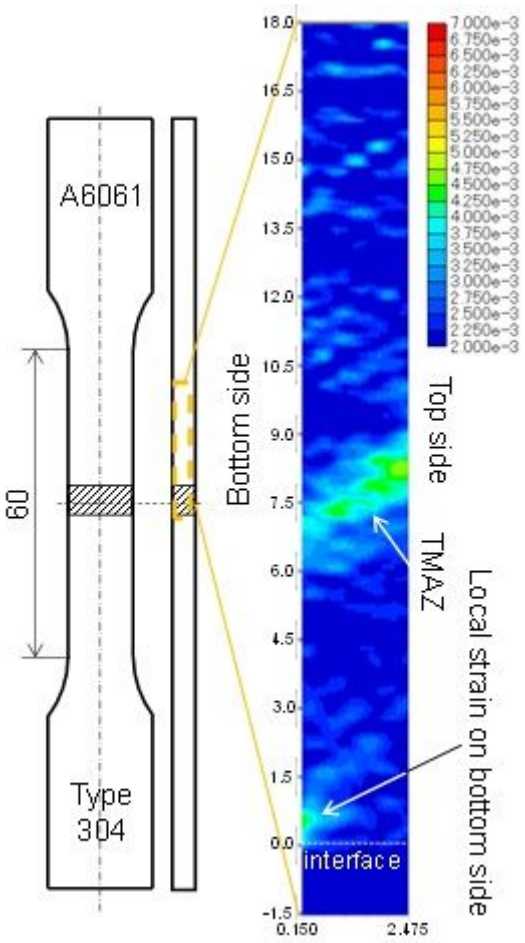

Figure 13

y-axis strain on the side surface at 6.0 kN.

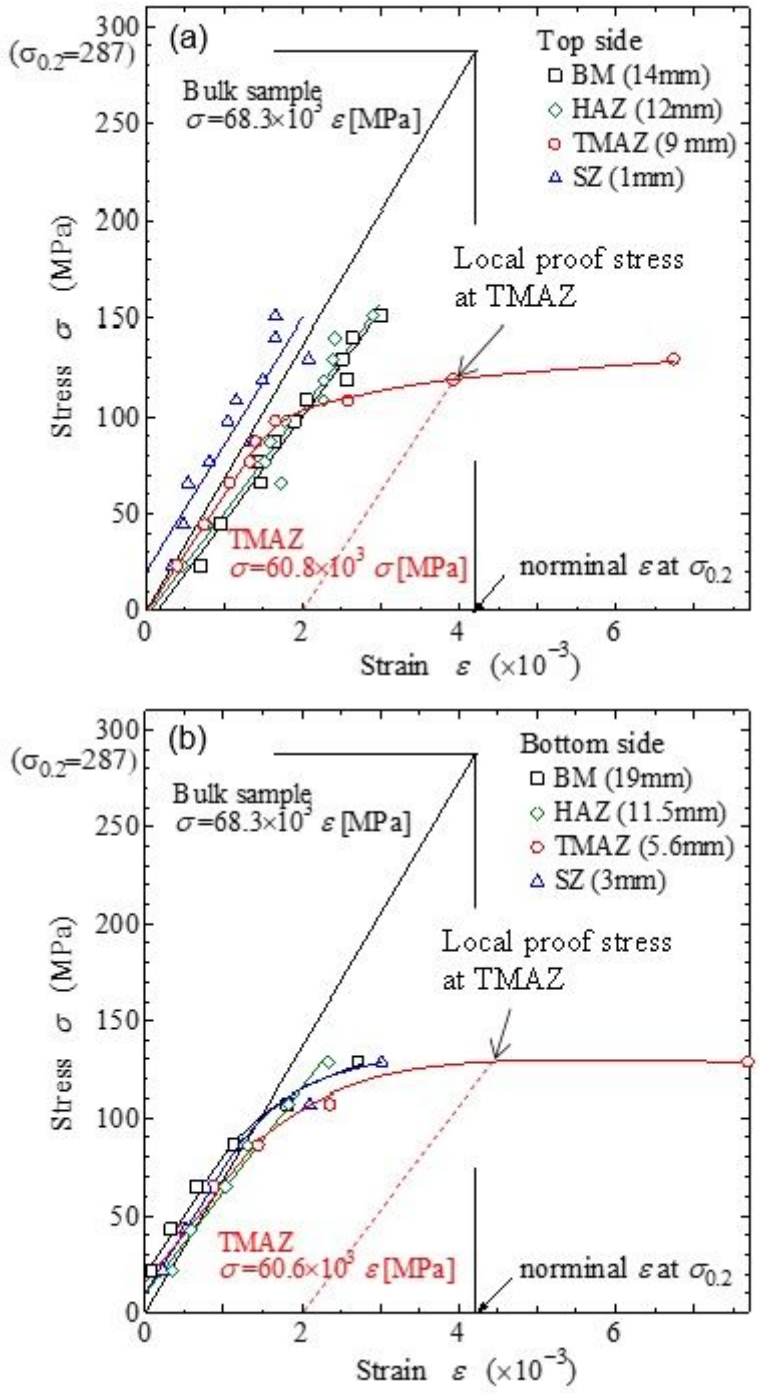

Figure 14

Local stress-strain behaviour: (a) Top side, (b) Bottom side.